Coordinated tuning of MMC-HVDC interconnection links and PEM electrolyzers for fast frequency support in a multiarea electrical power system

10

Georgios Giannakopoulos[a], *Arcadio Perilla*[a], *Jose Rueda-Torres*[a], *Peter Palensky*[a], *and Francisco Gonzalez-Longatt*[b]
[a]Department of Electrical Sustainable Energy, Delft University of Technology, Delft, Netherlands, [b]Department of Electrical Engineering, Information Technology and Cybernetics, University of South-Eastern Norway, Porsgrunn, Norway

10.1 Introduction

Power systems nowadays are experiencing a progressive increment of the power electronic interfaced (PEI) units in generation, transmission, and demand sides [1]. Power converters, especially voltage source converters (VSCs), are utilized to offer grid connection to renewable energy sources (RES), asynchronously interconnect power systems, transfer remotely large amount of power, and enable the introduction of responsive demand units into the grid [1]. The emerging grid transformation has significantly altered its dynamic behavior due to the low inertia conditions encountered, the lack of natural inertial response, the reduced short circuit capacity, and the limited or RES-dependent reserves leading to faster and more frequent dynamics and significantly affecting the stability margins of the system [2–4]. Among the various resulting stability issues encountered, frequency stability has been highlighted as one of the main concerns for the transmission system operators (TSOs) under the new operating conditions [5].

To cope with the new dynamic behavior of the system, PEI units should shoulder the frequency regulation and exploit the supporting capabilities of VSCs. For this reason, the adaptation and improvement of controllers attached to various elements such as wind turbines (WTs) [6–8], solar systems, energy storage systems (ESSs) [8–10], high voltage direct current (HVDC) interconnection links [11–13], and responsive demand units like electrolyzers [14–17] with the provision of ancillary services such as active power support has gained great attention lately. The effectiveness of the control schemes proposed strongly depends on the amount of active power injected/absorbed from these units following an imbalance and the ramp rate or active power gradient (APG) at which the injection/absorption takes place. The latter variables

Power System Frequency Control. https://doi.org/10.1016/B978-0-443-18426-0.00008-X

depend on the availability of the prime source behind the converter, the technical limitations of each unit, and its control structure and response to sensed deviations. Nowadays, very fast injection rates have been achieved from PEIs as an APG of 1000 MW/s has been reported in [18]. The influence of the power injection at very fast ramp rates has been considered in many grid code requirements as in the case of the UK increasing further the interest on their control techniques [19].

The incorporation, improvement, and coordination of the APG control scheme in the controllers of VSCs of various technologies aiming at fast active power—frequency support following commonly occurred active power imbalances is an ongoing research area. In [11], a preliminary research has shown the potential of rapidly modifying the power flows in a modular multilevel converter (MMC) based HVDC link asynchronously interconnecting two areas with different inertia levels against a critical active power imbalance. Similarly, in [17], the capability of fast frequency support (FFS) from responsive demand hydrogen-based units such as proton exchange membrane (PEM) electrolyzers using different strategies to control the amount and the rate of change of their consumption against frequency excursions has been investigated. Although the latter research has proven the effectiveness of the APG control scheme against significant frequency excursions, it has also highlighted potential coordination issues when the complexity of the system increases. In fact, in [11] the necessity of optimal tuning of the frequency controllers has been highlighted in a small system with 2 asynchronously interconnected areas of similar inertia level to achieve the optimal sharing of the imbalance according to the areas' characteristics and response. In [13], the complexity of the original system in [11] has been increased through the utilization of HVDC interconnectors and PEM electrolyzers in a simple small in size multienergy system against a significant active power imbalance. In the latter research, the necessity and complexity of coordinative tuning of the frequency controllers participating in the frequency regulation has been revealed, to avoid adverse control actions that may lead to insufficient or over frequency regulation. To solve this issue, authors in [12,13] have proposed two different methods to achieve a coordinated tuning of the frequency controllers in small and simple systems aiming at optimal sharing of imbalances among different supporting means. However, the optimal and coordinative tuning strategy of the APG control scheme in more complex and larger systems constitutes a challenging and still open research gap.

Going beyond the current state of art, this chapter focuses on a more complex situation, where the frequency regulation following a commonly occurred active power imbalance is simultaneously and coordinatively performed in a multiarea, hybrid HVDC-HVAC power system with multiple responsive demand units (i.e., PEM electrolyzers). This chapter aims to examine the effectiveness of the APG control scheme attached to the converters of MMC-based HVDC interconnectors as well as to multiple PEM electrolyzers installed at various locations of a complex multiarea, meshed system. Also, it gives insight into the optimal tuning of multiple frequency containment reserves (FCRs), which simultaneously regulate the system frequency. To this aim, an optimization problem, aiming at the minimization of the frequency excursions in all interconnected areas participating in the frequency regulation from their nominal value, is formulated. The problem is solved by using the mean-variance

mapping optimization (MVMO) algorithm. MVMO is a metaheuristic algorithm with proven effectiveness for solving computationally expensive and hard-to-solve optimization problems. The chapter reveals the importance of the location of installation of the various FCRs with respect to the location of the active power imbalance in a multiarea highly meshed power system. To reach these goals, a co-simulation environment between DIgSILENT PowerFactory (DPF) 2020 utilized for the modeling and simulation of the dynamic responses of the system and Python 3.8 used for the optimization problem definition and solution has been created.

The remainder of the chapter is structured as follows: Section 10.2 focuses on the modeling of the PEI elements such as MMC-based HVDC links and PEM electrolyzers and its controllers for dynamic stability studies. In Section 10.3, the problem formulation of the optimization problem is presented. In Section 10.4, the MVMO algorithm utilized for solving the optimization problem is briefly explained. In Section 10.5, a detailed description of the test system, and the modifications applied to it, are provided. Finally, Section 10.6 presents an analysis of the results obtained from the simulations.

10.2 Theoretical background

10.2.1 Modeling and control of the MMC-HVDC links

One of the goals of this chapter is to introduce MMC-based HVDC interconnection links with the provision of FFS among the areas of a multiarea system enabling their electromagnetically decoupled, asynchronous interconnection. The modeling of such a link consists of the representation of the MMC converter stations, the DC cables, the interface with the grid, and the control system of the converters [20]. The level of detail of the models depends on the time frame the phenomena of interest occur and thus for dynamic stability studies and root mean square (RMS) simulations of interest, it refers to a time frame of ms to s [21].

In literature, several different models embodying the behavior of the MMC converter station have been proposed [22]. In this research and according to the guidelines of CIGRE in [21], an average value model (AVM) type 6 developed by DIgSILENT GmbH [20] suitable for dynamic stability studies has been utilized and can be observed in Fig. 1. In this type of model, the switching actions of the insulated gate bipolar transistors (IGBTs) and the diodes representation are neglected and thus the AC side of the converter is represented as a fully controllable voltage source and the DC side of the converter as a fully controllable current source in parallel to an equivalent capacitance representing the total submodules' (SMs') capacitance [21]. Also, with respect to [23], the arm reactor is considered at both sides increasing the accuracy of the model. The output of the converter stations is assumed to be perfectly sinusoidal and thus no harmonic injection is encountered into the grid, whereas all internal variables are assumed to be perfectly controlled so that the SMs capacitors' voltages are balanced and second harmonic circulating currents are suppressed [20,21].

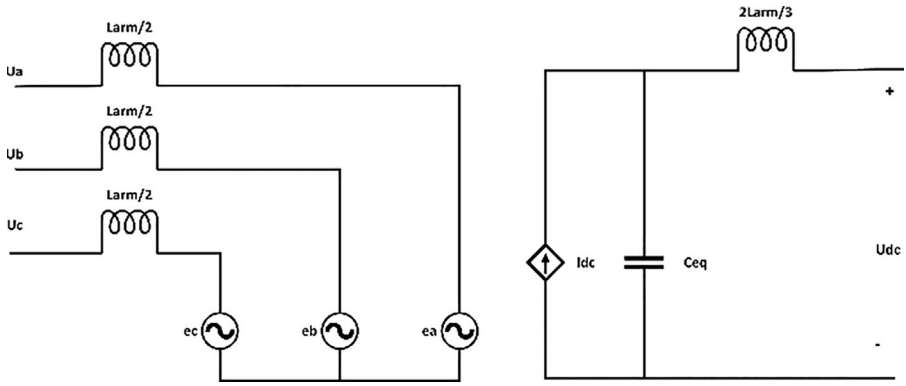

Fig. 1 Equivalent schematic diagram of MMC converter stations of the HVDC links.

As far as the interconnection of the converter stations is concerned, on the DC side, it is facilitated by DC cables represented by their lumped equivalent Π (PI) model connected in a bipolar configuration, the most preferable one for HVDC interconnection link applications [24]. On the AC side, the converters are connected to the local AC networks via transformers and inductors of suitable power and voltage ratings able to offer smooth interconnection to the grid and limit large fault currents. The complete representation of MMC-based HVDC link in DPF 2020 can be observed in Fig. 2.

The output of the MMC stations in an HVDC link depends on the switching actions of the converters, which are controlled typically through sinusoidal PWM modulation [25]. To produce the reference voltages for the PWM modulation, the current vector control strategy used in many applications and presented in [26] has been deployed. According to this principle, the active and reactive power output of the converters can be independently controlled with the aid of a phase lock loop (PLL) device and the Clarke-Park transformation. The voltage reference for the PWM modulation is generated within a fast inner current control loop by comparing in PI controllers the measured currents on the output of the MMC station transformed into the dq frame with current reference signals (id_ref) and (iq_ref) generated in an outer control loop to control the active and reactive power output, respectively. The id_ref is generated

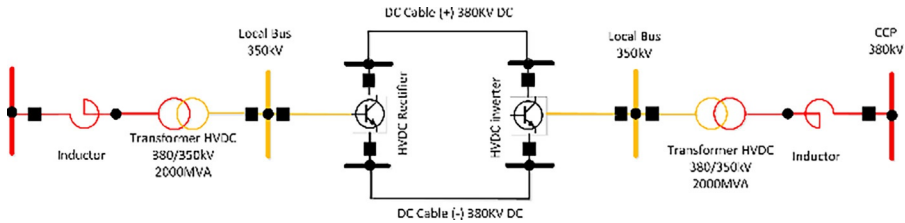

Fig. 2 MMC-based HVDC interconnection link schematic diagram.

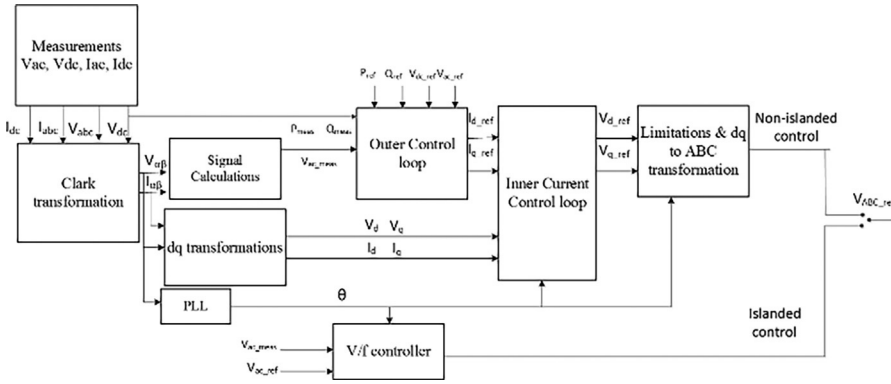

Fig. 3 MMC station control structure based on current-vector control.

in the active power outer controller (P/V_{DC} controller) with respect to an active power setpoint (P_{AC_ref}) or with respect to a DC voltage setpoint (V_{DC_ref}) and the iq_ref is generated in the reactive power outer controller (Q/V_{AC} controller) either with respect to a reactive power setpoint (Q_{AC_ref}) or to an AC voltage setpoint (V_{AC_ref}) [27]. The complete control structure of the converter stations of the MMC HVDC links can be observed in Fig. 3 and is further explained in [20,21].

In this study, the control of the active power output of all the inverter stations installed at the receiving ends of the HVDC links is controlled with respect to an active power setpoint (P mode), whereas all the rectifiers installed in the sending ends of the HVDC links are controlled with respect to DC voltage setpoints (V_{DC} mode) to maintain the active power balance on the DC side of the HVDC links. Reactive power control is performed at both ends of the HVDC links with respect to reactive power setpoints provided by the load flow solution.

Additionally, in this chapter, the control of the active power output of the MMC station has been further enhanced with the APG control scheme inspired by [11–13] to respond to frequency excursions encountered in the interconnected AC networks. For this reason, the P/V_{DC} controller of all the inverter stations has been modified as observed in Fig. 4 to contain the APG activation block shown in red. The latter one can adjust the active power setpoint (P_{AC_ref}) by ΔP and also the rate at which this change is applied through the APG parameter of the rate limiter. In that way, the degree and the rate of change of the active power output of each HVDC link participating in the frequency regulation can be controlled to provide FFS. The selection of the parameters ΔP and APG is based on the solution of an optimization problem formulated in Python according to the frequency responses of the interconnected areas participating in the frequency regulation aiming at improved responses and optimally shared imbalances. Finally, the change in the power flows of the HVDC links is performed once per simulation considering an activation and actuation delay of 0.3 s following any imbalance and all the technical limitations of each of the MMC-based HVDC links considering the maximum power transfer capability of the link according to its rated capacity and the maximum ramp rate it can handle according to the limits in [13].

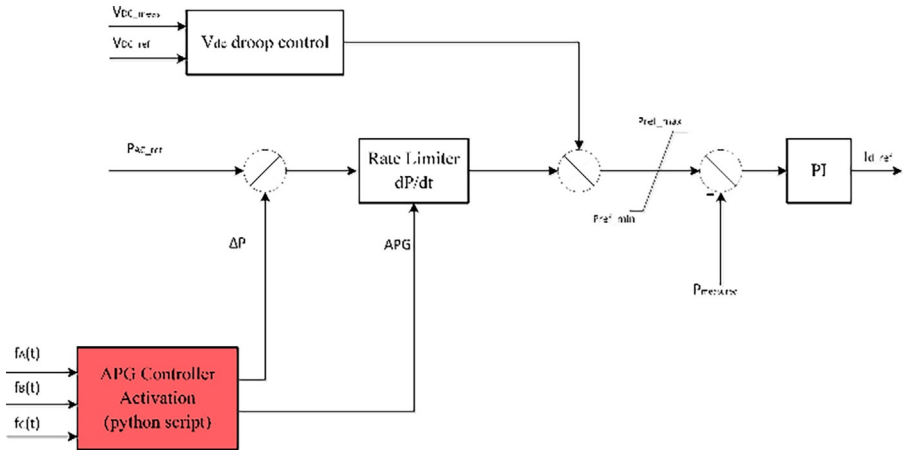

Fig. 4 Modified P/V_{DC} controller of the MMC-HVDC link with the APG control strategy.

10.2.2 Modeling and control of PEM electrolyzers

A second goal of this research is to introduce to the power system hydrogen-based responsive demand units such as electrolyzers with the provision of FFS by rapidly modifying their consumption utilizing the APG control strategy when active power—frequency imbalances occur. Hydrogen-based demand units have gained great attention recently due to their capability to operate as green and efficient energy carriers in many applications [14]. In fact, according to [28], it is expected that by 2050 hydrogen-based units will overcome the 18% of the total demand. Among the different types of electrolyzers developed, PEM electrolyzers have shown high potential of applicability in large-scale grid applications due to their low financial expenses and efficient dynamic performance in combination with their technical characteristics, such as high current density, high hydrogen purity, efficiency levels, and compact design [15,29]. Also, according to [16], PEM electrolyzers exhibit very fast dynamic response to setpoint changes of their active power consumption, constituting them a FCR of high significance for grid applications. For these reasons, PEM electrolyzers are the type of hydrogen-based demand units considered in this study.

The modeling of large-scale PEM electrolyzers for grid applications constitutes a challenging task, due to the lack of existing large-scale applications. Various studies have proposed different models focusing on different characteristics according to the research needs, utilizing the parallel interconnection of modular, smaller in size units [30]. From the electrical point of view, the complete representation of an electrolyzer consists of i) the electrolysis stack, ii) the balance of plant (BoP), and iii) the electrical conversion system [15]. A schematic diagram of the complete representation of PEM electrolyzer can be observed in Fig. 5.

However, as explained in [16], for power system stability studies the main parameter of interest is the ramp rate at which the consumption of the electrolyzer changes with respect to setpoint changes. For this reason, in this chapter, a simplified, yet

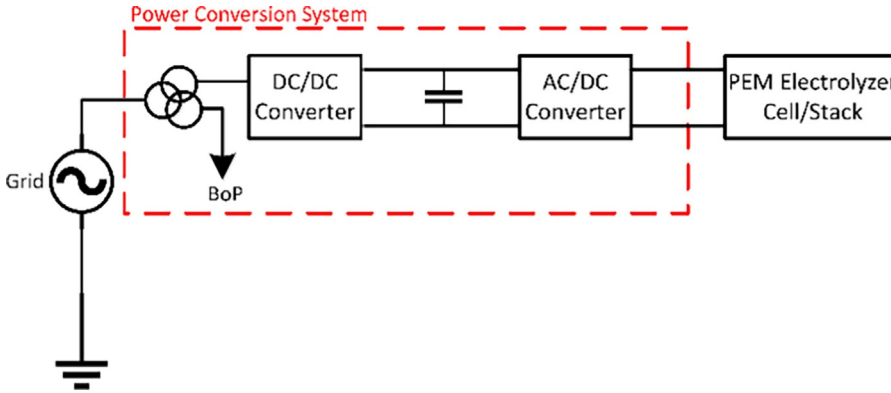

Fig. 5 PEM Electrolyzer's complete representation.

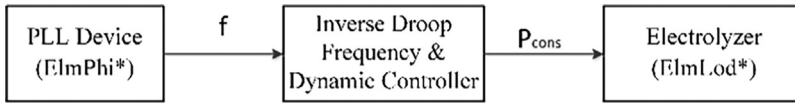

Fig. 6 PEM Electrolyzer's model in DIgSILENT PowerFactory.

accurate representation has been considered and can be observed in Fig. 6. In this model, the electrolyzer is modeled as a general load with no self load-frequency regulation capability operating at 20 kV and being connected to the local grid via a step-up transformer plus its associated dynamic—frequency control model in a structure, as shown in Fig. 7. In this way, the PEM electrolyzers are isolated from the grid and their response to active power setpoint changes can be effectively represented.

As far as the control structure of the electrolyzer implemented in this study is concerned, it is characterized by the dynamic controller and a frequency controller enhanced with the APG strategy. The dynamic response of the electrolyzers to active power setpoint changes according to [15,16,30] is linear and typically has a ramp rate of approximately 0.5–2.5p.u./s and thus it is represented by an externally controllable

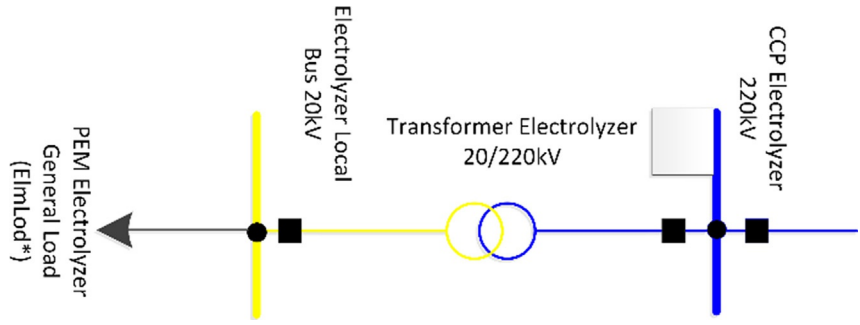

Fig. 7 PEM electrolyzer's control structure.

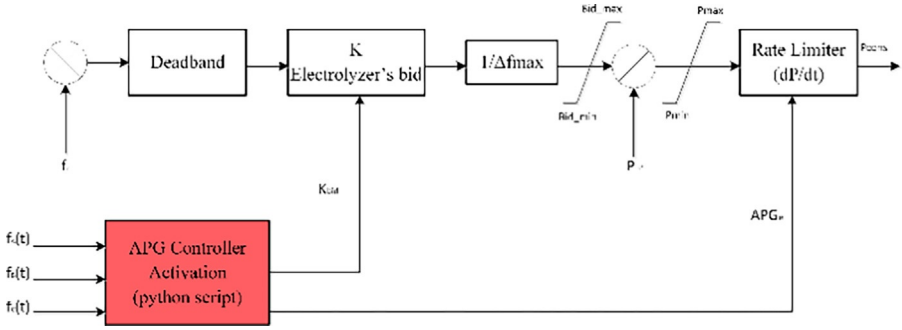

Fig. 8 PEM Electrolyzer's frequency-dynamic controller block diagram.

rate limiter operating with respect to the installed capacity of each unit. Then an inverse droop frequency controller is used to alter the nominal consumption of the electrolyzer with respect to sensed frequency excursions. The parameter selection of the various blocks included in the frequency controller have been selected according to the FCR regulations in [31] (Deadband = 10 mHz, $\Delta f_{max} = 200$ mHz). Furthermore, it has been assumed that these units can offer FFS continuously and for an unlimited amount of time, but the consumption of the unit should never fall below 30% of its rated capacity and should not overcome 100% of its rated capacity according to [16,17]. In addition, as observed in Fig. 8, the frequency controller has been enhanced with the APG control scheme so that the bid provided, and the ramp rate of the consumption is externally controlled through a Python script defining and solving an optimization problem that simultaneously tunes the control parameters of the frequency controllers of FFS means aiming at the minimization of the frequency deviations in interconnected areas participating in the frequency regulation. Finally, according to the technical limitations of each unit, the bid and the ramp rate of each electrolyzer are maintained within the acceptable values analyzed in [16,17].

10.3 Optimization problem formulation

In cases FFS is going to be provided simultaneously by various FCRs such as PEM electrolyzers and MMC-based HVDC links taking advantage of the APG control scheme, coordinative tuning of the controllers is more than necessary. In fact, if no means of communication are utilized to offer a coordinative response, adverse control actions leading to insufficient or over regulation of the frequency may be encountered. To tackle this problem, in this study, an optimization problem has been formulated aiming at a coordinative tuning of the frequency controllers of the FCRs participating in the frequency regulation when an active power imbalance occurs in one of the interconnected areas. In that way, the controllers are properly tuned so that the corresponding FCRs can provide the necessary amount of active power in the required rate to achieve the optimal frequency response in the affected area and the minimum impact on the neighboring areas and thus achieving the optimal share of the imbalance

according to their characteristics, the reserves availability, and the inertia level of each area without any means of communication.

In this study, a multiarea test system has been considered with areas being electromagnetically decoupled through MMC-based HVDC links. Hence, each area is characterized by its own frequency that needs to be preserved within the acceptable normal operating state limits set by TSOs explained in [32,33]. In case of an active power imbalance in one of the interconnected areas, if the MMC-HVDC links are activated to provide FFS, as explained in Section 10.2, the power flows in the tie-lines among the areas change, resulting in active power imbalances in the supporting areas sensed at the CCP of the HVDC link.

Taking all the above into consideration the proposed problem formulation aims at the minimization of the frequency excursions in all the k interconnected via MMC-based HVDC links areas participating in the frequency regulation from the nominal value of each one of them. Mathematically, this can be formulated as follows:

Minimize

$$\mathrm{OF}(\mathbf{x}) = \int_0^{\tau} w_A(f_A(\mathbf{x},\ t) - f_{nA})^2 + w_B(f_B(\mathbf{x},\ t) - f_{nB})^2 + \ldots + w_k(f_k(\mathbf{x},\ t) - f_{kA})^2 \tag{1}$$

Subjected to

$$\mathbf{x}_{\mathbf{min}} \leq \mathbf{x} \leq \mathbf{x}_{\mathbf{max}} \tag{2}$$

where w_i is a weighting factor which in this chapter has been set equal to 1 in order not to prioritize the frequency response of an area over the other, f_i is the instantaneous frequency of the ith area in Hz measured at any bus of the area, and f_{ni} is the nominal value of the frequency of the ith area in Hz. The optimization vector $\mathbf{x}$ contains 2 optimization variables for each of the FCRs activated to participate in the frequency regulation and varies in size according to the number of installed and actively operating FCRs. For the MMC-based HVDC links, the optimization variables are the additional active power ΔP_j that will be provided by the jth HVDC link and the $\mathrm{APG_j}$ which is the rate at which the change in the active power reference is applied in the $\mathrm{P/V_{DC}}$ controller of the inverter of the jth HVDC link as observed in Fig. 4. For each of the PEM electrolyzers, the optimization vector contains two variables, the bid of the wth electrolyzer, $K_{\mathrm{bid}w}$ and the ramp rate of its consumption, $\mathrm{APG_{ew}}$. As a result, in case of a system with a single MMC-based HVDC link and a single PEM electrolyzer participating in the frequency regulation, the optimization vector contains four optimization variables and is formulated as follows:

$$\mathbf{x} = [\Delta P_i,\ \mathrm{APG_i},\ K_{\mathrm{bid\,w}},\ \mathrm{APG_{e_w}}] \tag{3}$$

Each of the optimization variables remains bounded within the acceptable values according to the technical limitations of each unit. For the MMC-based HVDC links,

the maximum active power transfer capability of each link and the maximum acceptable ramp rate the link can handle should be considered, whereas for the PEM electrolyzers the optimization variable should consider the maximum allowed bid provided by the electrolyzer for frequency support and the maximum ramp rate each unit can handle. In this study, the boundaries have been selected according to [13] for the MMC-based HVDC links and [17] for the PEM electrolyzers and can be observed in (4) to (7).

$$0 \leq \text{APGi} \leq 60 \tag{4}$$

$$0 \leq P_{\text{refi}} + \Delta P_i \leq P_{\text{rated}_i} \tag{5}$$

$$0 \leq K_{\text{bid}_w} \leq 0.7 P_{\text{elec}_{\text{rate}_w}} \tag{6}$$

$$0 \leq \text{APG}_{ew} \leq 0.5\, P_{\text{elec}_{\text{rated}\,w}} \tag{7}$$

The objective function (OF) calculated in (1) takes into consideration the frequency excursions in all interconnected areas with MMC-based HVDC links participating in the frequency regulation and tries to minimize the excursions throughout the whole simulation period aiming at improved rate of change of frequency (RoCof), maximum instantaneous frequency deviation (frequency nadir), and steady-state frequency deviation in the affected area where the active power imbalance occurs and the minimum impact on the other areas. According to the frequency responses of each area, it can control the participation of the HVDC links and the PEM electrolyzers in the frequency regulation according to their supporting capabilities, their location of installation, and the characteristics of their responses. It is also easily applicable in any type of system as the instantaneous frequency of each area required for the calculation of (1) can be measured at any bus of the corresponding area.

10.4 The mean variance optimization algorithm

The mean variance optimization algorithm (MVMO) is a representative member of the family of metaheuristic evolutionary algorithms able to deal with computationally expensive optimization problems within a short number of fitness evaluations, achieving results of high quality and fast convergence rate [12,13,34]. For this reason, in this study, it has been utilized to effectively solve the optimization problem formulated in Section 10.3 and coordinatively tune the frequency controllers of the FCRs installed at various locations of the test system against commonly occurred active power imbalances. In this study, both the optimization problem and the MVMO algorithm have been formulated in Python 3.8 and operate in a co-simulation environment with DPF 2020 to perform a series of RMS simulations, the results of which are used as inputs to execute the fitness evaluations, i.e., the calculation of (1) within the algorithmic process.

As observed in Fig. 9, at an initial state, an initial solution vector $\mathbf{x_0}$ is either provided by the user or is randomly generated by the algorithm based on the available

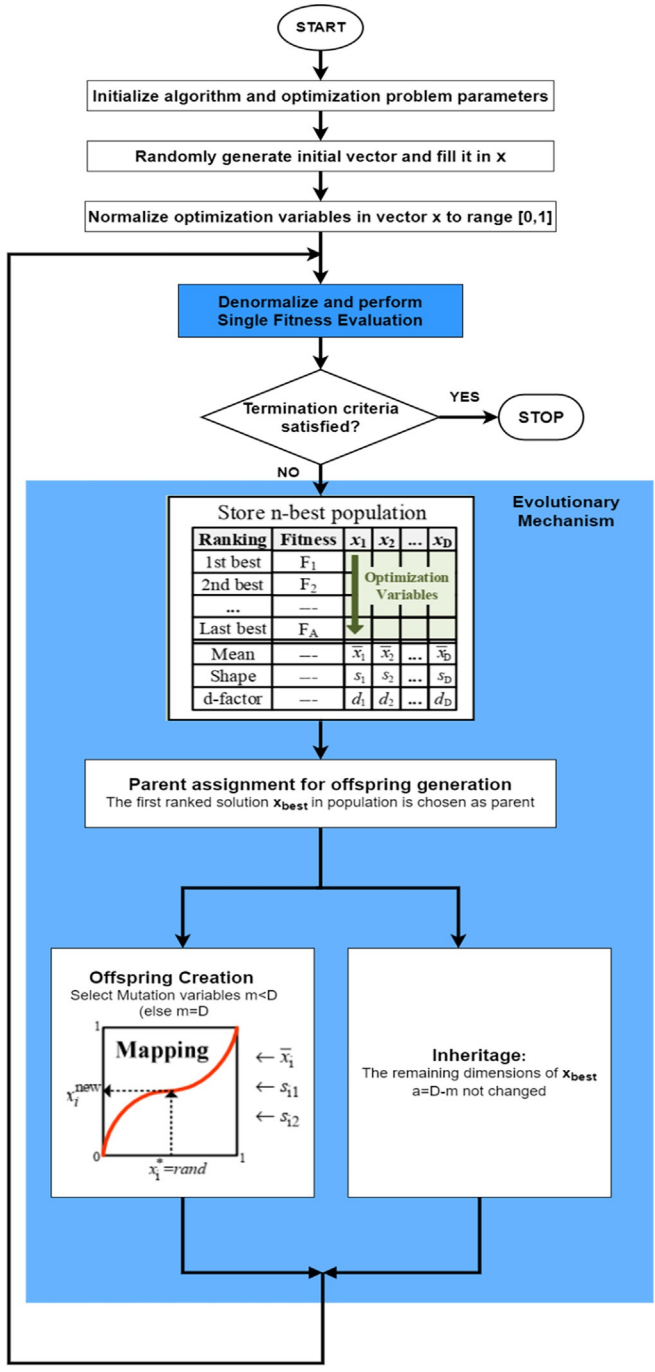

Fig. 9 The MVMO algorithmic process.

research space. The initial vector or any other candidate solution vector is normalized from the [min,max] range of each optimization variable to a [0,1] range. In that way, any offspring solution generated by the MVMO algorithm has its optimization variables within the acceptable bounds and no further actions need to be taken to correct the solution or penalize the OF value. Hence, the algorithm can perform and converge within a shorter period. In the next step, the candidate vector $\mathbf{x_0}$ is denormalized, and its variables are applied in DPF through Python in the corresponding HVDC links and PEM electrolyzers.

Then RMS simulation is performed in DPF, and the corresponding frequency responses of the system are obtained from the python-based MVMO as inputs for the calculation of the OF, i.e., the fitness evaluation. According to the results of the fitness evaluation, an archive is used to store the best solutions achieved throughout the iterations, the corresponding optimization vectors $\mathbf{x}$ and statistical data such as the mean, the variance, and shape factors calculated for each of the optimization variables. Then the MVMO can generate an offspring solution based on the best parent solution achieved so far with the guidelines of a mapping function which is able to provide the direction of evolution of each optimization variable according to the input statistical data of each variable. The iteration process continues until the termination criteria have been fulfilled and a final solution vector is extracted from the algorithm achieving the optimal tuning of the frequency controllers of the FCRs participating in the frequency regulation. Further details about the MVMO algorithm, the calculation and selection of its parameters and the mapping function can be found in [34]. Fig. 10 also describes the co-simulation process between DPF and Python for the solution of the optimization problem and the tuning of the frequency controllers.

In this study, the MVMO algorithm has been selected to terminate after a predefined number of fitness evaluations equal to 100 is performed. The latter number of iterations has been proven to be enough to reach a local optimum solution and tune in an acceptable, fast, and efficient manner the controllers. At an initial state, all statistical metrics are maintained equal to 0.5 to utilize better the available research space as explained in [13]. Initial vectors may be provided based on expected results and boundaries have been selected according to the technical limitations of each unit as explained in Sections 10.2 and 10.3. Finally, in this study, no further constrains have been applied in the evolution of the optimization variables, the archive has a constant size of 5, and the optimization vector is mutated at its full extend.

10.5 The test system

To evaluate the effectiveness of the coordinated APG control strategy proposed in this chapter, a multiarea test system, the original PST 16 benchmark system designed for power system stability (PSS) studies has been used as a starting point. The original system consists of three meshed areas interconnected by long and weak HVAC tie-lines which have to facilitate the transfer of large amount of power. The system operates at three transmission voltage levels of 110 kV, 220 kV and 380 kV and has 16 synchronous generating units (SGUs) widely spread across the three areas. The

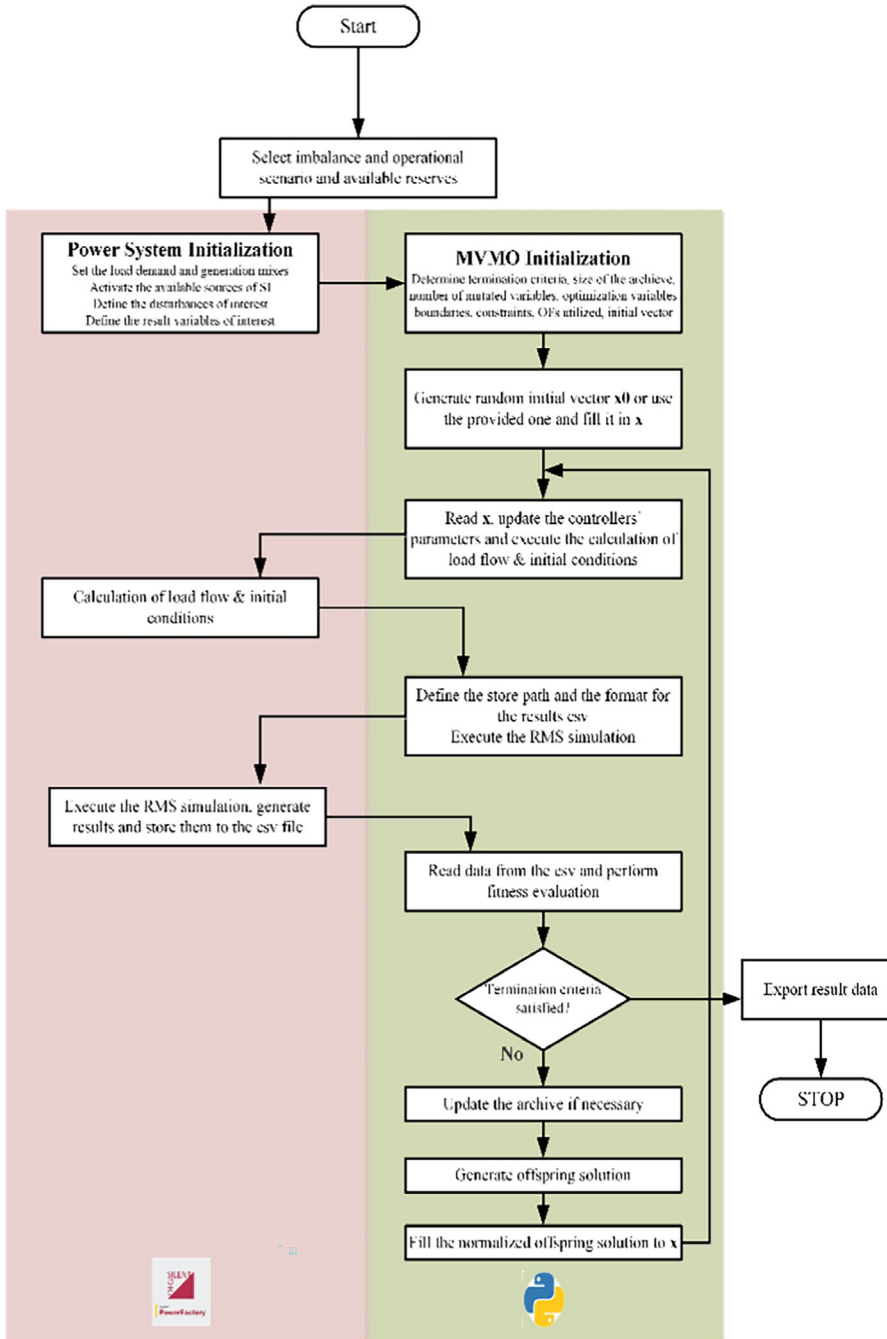

Fig. 10 Co-simulation process flowchart.

parameters of the system have been chosen according to real parameters of the European System aiming at realistic scenarios. Additionally, the system has been designed to operate at multiple demand scenarios according to the expected demand throughout the year. Further details about the original PST 16 benchmark system can be found in [35,36].

In this study, the original PST 16 benchmark system has been modified to facilitate the integration of MMC-based HVDC links and PEM electrolyzers so as to form a multi-area, hybrid HVAC-HVDC power system with responsive demand units, i.e., PEM electrolyzers. The models of all the elements have been designed to offer the necessary accuracy for dynamic stability studies of interest. The modified system comprises of 16 SGUs installed at the same buses with the original system consisting of multiple parallel units with power ratings of 220 MVA, 247 MVA, and 259 MVA operating at 15.75 kV and being connected to the grid via power transformers of suitable power rating and voltage ratios. The system has been selected to operate at medium loading conditions and thus the total generation is equal to 10.3 GW. The modeling of the SGUs has been done according to the fifth order model suitable for PSS studies as explained in [37,38] and its control structure contains the basic control blocks described in [39], an excitation system, a speed-governing system, and a power system stabilizer. In fact, for the representation of the latter control blocks, the IEEE AC4A excitation system model and the IEEEG1 speed governing system, being the most commonly used ones for conventional SGUs and PSS studies have been considered. The modeling and the parameter selection for these blocks has been performed according to the guidelines provided in [40,41], respectively. The power system stabilizer has been modeled with respect to a simple representation analyzed in [36]. The optimal tuning of the power system stabilizer and the introduction of secondary frequency control schemes are out of the scope of this study, and, thus, it has not been considered. Finally, the selection of the parameters of the SGU model in DPF has been done based on the data provided by the original PST 16 system in [35].

On the demand side, the total consumption of the system is equal to 10.2 GW consisting of conventional general loads and PEM electrolyzers. In fact, 20% of the load demand of each area of the original system has been replaced by PEM electrolyzers of the same power need. The latter was based on the expected scenario of 2050 presented in [28]. Hence, in total 11 electrolyzers have been installed, 3 in area A, 4 in area B, and 4 in area C representing the 20% of the demand of each area and can be observed with the green triangle in Fig. 11. The representation of the PEM models has been facilitated according to Section 10.2. The location of installation of the PEM electrolyzers has been considered to be constant at different system points such as close to the CCPs of the HVDC links, close to SGUs and remote points to evaluate any possible relation between their location of installation with respect to the disturbance.

Additionally, the original PST 16 benchmark system has been modified to facilitate the integration of MMC-based HVDC links presented in Section 10.2. In fact, the HVAC tie-lines between the 3 areas have been replaced by MMC-based HVDC links of 2000 MVA operating at 350 kVAC and 380 kVDC on a bipolar configuration. Transformers of suitable power rating and voltage ratio have been utilized to smoothly

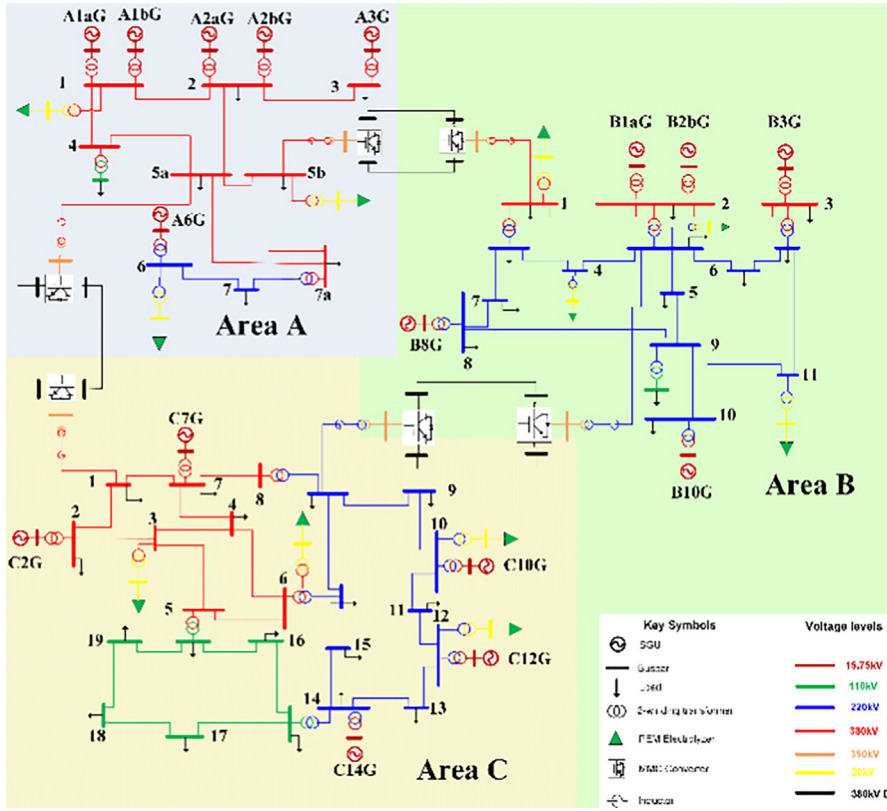

Fig. 11 The modified PST 16 benchmark system.

interconnect them to the CCP of each area either at 220 kV or at 380 kV. The MMC inverter stations have been set in P-Q control mode, whereas the MMC rectifier stations in V_{DC}-Q control mode with respect to active and reactive power setpoints provided by the load flow solution before the introduction of the HVDC links. In that way, the three areas are effectively electromagnetically decoupled and characterized by a different frequency, whereas the expected tie-line power flows between the areas are preserved.

The PEI units installed, i.e., MMC-based HVDC links, and PEM electrolyzers have been enhanced with the APG control strategy as explained in Section 10.2 to be able to respond to sensed frequency excursions. Also, for the voltage, current, power, and frequency measurement and for synchronization reasons, measurement devices, and phase lock loop devices have been installed at the CCPs of the MMC-based HVDC links, the DC buses of the MMC stations, and the CCPs of the electrolyzers with the grid.

Having introduced the new elements, a schematic diagram of the modified PST 16 benchmark system can be observed in Fig. 11. The modified system consists of three electromagnetically decoupled areas each of which has a constant frequency at 50 Hz during steady-state conditions as the generation-demand active power balance is

Table 1 Modified PST 16 system—element distribution.

	SGUs	AC buses	DC buses	Trafos	General load demand	PEM electrolyzers	AC transmission lines	DC cables	MMC stations
Area A	6	20	–	11	8	3	11	–	–
Area B	5	24	–	13	11	4	14	–	–
Area C	5	32	–	13	17	4	24	–	–
HVDC links	–	12	12	6	–	–	–	6	6
Total	16	88	12	43	36	11	49	6	6

Table 2 Generation and load demand in the modified system.

	Generation (MW)	Demand (MW)
Area A	3150	1770
Area B	4000	4670
Area C	3130	3705
Total	10280	10145

preserved with the aid of the local SGUs and imports/exports from the HVDC links. Also, all the bus voltages and equipment loading are preserved within the normal operating limits and thus the load flow solution successfully converges. Area A is a mainly exporting area as it provides 600 MW to area B and 700 MW to area C, whereas area C provides also 100 MW to area B. Detailed information about the element distribution and the generation-demand profiles of each area can be observed in Tables 1 and 2, respectively. Each of the three areas has a different inertia level based on the local SGUs and different reference machines compared to the original system. In area A, A1aG is the reference SGU, and its inertia is equal to 6.9093 s, in area B, B10G is the reference machine, and its inertia is equal to 10.052 s and finally in area C, C7G is the reference unit and its inertia is equal to 6.9999 s. As a result, as expected the area with the lowest inertia level, area A, experiences the largest RoCof, frequency nadir and steady-state deviation for an active power imbalance of the same size (600 MW) applied to each of the three areas as observed in Fig. 12. Based on the aforementioned, it can be concluded that the modified system can be effectively used as a benchmark multienergy, multiarea, hybrid HVDC/HVAC power system for frequency stability studies.

10.6 Simulation study and results

10.6.1 Simulation method and workflow

The goal of this study is to evaluate the frequency response of a complex multiarea hybrid HVDC/HVAC power system when multiple elements such as HVDC links and PEM electrolyzers enhanced with the APG control strategy provide

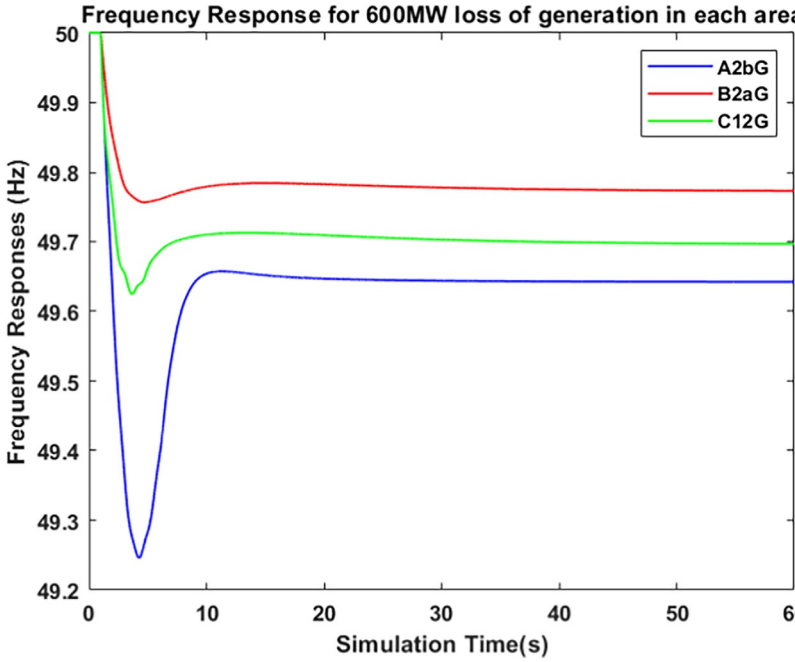

Fig. 12 Areas' frequency response for a 600 MW loss of generation.

simultaneously active power-frequency support against a commonly occurred active power imbalance. In this type of study, the time frame of interest is from ms to several seconds and thus this work was conducted based on time domain RMS simulations. The latter ones are performed on DPF 2020 considering a simulation time of 60 s and a time step of 0.001 s to capture the dynamic phenomena of interest. The definition, execution, and solution of the optimization problem described in Section 10.3 required for the coordinative tuning of the frequency controllers of the FCRs have been developed in Python 3.8 operating in a co-simulation environment with DPF.

The workflow of the simulation study as observed in Fig. 10 starts with the definition of the operating scenario of the system. This refers to the generation and demand conditions, which in this case have been assumed to be constant as described in Section 10.5, and the determination of the available active power frequency reserves that will participate in the frequency regulation. In this study, different scenarios considering different groups of available reserves have been defined and will be explained in B. In the next step, a commonly occurred active power imbalance, such as a loss of a significant SGU, is defined as a simulation event applied on the 1st s of the simulation to evaluate the system response. Having initialized the power system in DPF, the process continues with the initialization of the MVMO algorithm by defining the size of the optimization vector ($\mathbf{x}$) according to the availability of the FCRs, the termination criteria (number of fitness evaluations), providing an initial optimization vector ($\mathbf{x_0}$), setting the number of mutated variables and the size of the archive, and

defining the boundary conditions for each of the optimization variables. In this study, the optimization vector contains two optimization variables for each of the available FCRs one affecting the active power setpoint of the corresponding unit and one affecting the ramp rate of the active power output of the reserve. The boundary conditions of each unit are selected based on the technical limitations of each unit as described in (3) to (6) and a predefined number of 100 fitness evaluations is performed before exiting the iterations loop. The size of the archive is constant and equal to 5, whereas it has been assumed that all optimization variables are mutated throughout the simulation process.

Throughout the simulation, a candidate optimization vector contains the control parameters of the participating HVDC links and PEM electrolyzers. These parameters are modified in DPF accordingly through the Python script, and an RMS simulation is executed in each iteration. The results of the RMS simulation containing the frequency responses of the system areas are extracted in a csv file in a form readable by Python. The latter responses are imported to the Python script and are used for the calculation of the OF in (1). If the result of the fitness evaluation is better than the last evaluation stored in the sorted archive, then it takes its place with the corresponding optimization vector. In each case, the statistical data of each optimization variable (mean, variance, and shape factors) are updated and used from the mapping function to provide the evolution guidelines for the offspring solution vector. A new offspring solution is generated until the termination criteria is reached. When the loop ends, the optimum solution vector $\mathbf{x}$ that achieved the best frequency responses of the system areas is obtained along with the plots revealing the evolution of the OF and optimization variables values throughout the iterations.

10.6.2 Simulation Event and Operational Scenarios

The test system considered in this study, presented in Section 10.5, consists of three electromagnetically decoupled areas. This means that an active power event occurring in an area mainly affects the area of occurrence depending on its generation, inertia, and reserve characteristics and the operating conditions of the equipment at the time of the occurrence of the disturbance. The neighboring areas are only affected if the MMC-based HVDC links are activated to provide FFS. A typical active power imbalance that may occur in a power system leading to extensive frequency deviations is the loss of a significant SGU. For this reason, in this study, a series of RMS simulations has been performed in order to determine the loss of the SGU that causes the most significant active power imbalance in each area. In that way, the most critical imbalance can be selected as an indicative simulation scenario at which the effectiveness of the tuning method proposed can be evaluated. The frequency responses of the areas when each of the 16 existing SGUs is set out of operation on the 1st s of simulation without the activation of any synthetic inertia FCR can be observed in Fig. 13.

As it is observed the loss of the largest generating unit in area A, SGU A1aG, leads to the most significant frequency excursions reaching a nadir of 48.8 Hz that stabilizes at 49.5 Hz. Also, it can be observed that the loss of other large SGU in the same area also lead to extensive frequency deviations as area A has the lowest inertia conditions

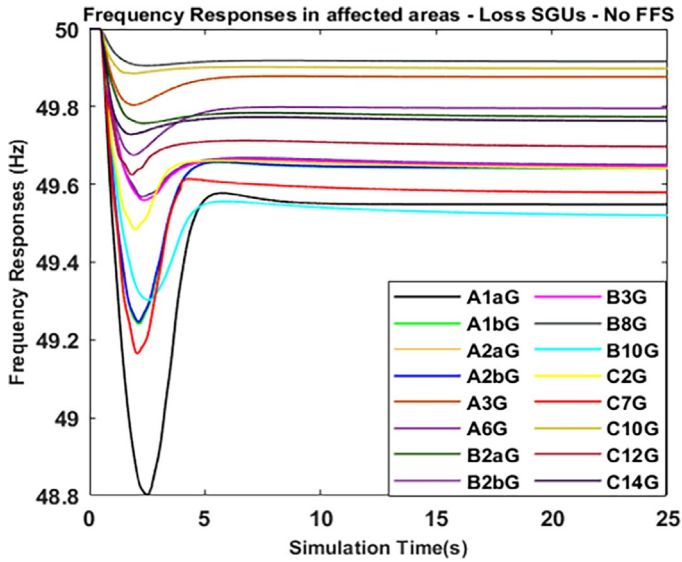

Fig. 13 Frequency responses in affected areas in loss of SGUs.

compared to other areas and acts as a main area for exports. Also, as expected in the other areas the loss of their largest SGUs such as C7G and B10G lead to frequency deviations out of the normal operating state limits according to the synchronous inertia levels of each area. For this reason, the loss of SGU A1aG, an active power event of 750 MW, is considered as the simulation event of this study occurring at 1 s.

Apart from the parameter event, different scenarios with respect to the availability of FCRs have been considered according to possible combinations. In that way, the importance of different FCRs according to their characteristics, limitations and location can be revealed. The different simulation scenarios can be observed in Table 3. In Scenario 1, only the local SGUs in the affected area are providing their support. In Scenario 2, local PEM electrolyzers in area A inject at the maximum ramp rate different amount of active power according to their available bid. Bids of 30%, 50%, and 70% of their rated capacity have been considered. In Scenario 3, the imbalance is shared among the three interconnected areas via the HVDC links trying to mitigate the frequency excursions in area A with the minimum impact on the neighboring

Table 3 Simulation scenarios.

Active FCRs	SGUs	Local PEM in affected area	HVDC links	PEM in supporting areas
Scenario 1	YES	NO	NO	NO
Scenario 2	YES	YES (different bids)	NO	NO
Scenario 3	YES	NO	YES	NO
Scenario 4	YES	YES	YES	YES

areas. Electrolyzers are not participating in this scenario and thus the optimization vector **x** contains six optimization variables in total optimized with the aid of the MVMO algorithm trying to minimize the value of OF in (1). Finally in Scenario 4, all available FCRs installed, HVDC links, and PEM electrolyzers in all areas are cooperatively tuned against the same imbalance according to the results of MVMO algorithm trying to minimize OF in (1). In that case the optimization vector contains 28 optimization variables as explained in Section 10.3.

10.6.3 Optimization results

10.6.3.1 Scenario 1

In case no FFS is provided by any means of synthetic inertia in the affected area, the frequency response of area A when the SGU A1aG is set out of operation depends only on the remaining SGUs of area A and the characteristics of their speed-governing systems. The frequency responses of the interconnected areas can be observed in Fig. 14. As it is clear, the frequency drops rapidly at a rate of 0.32 Hz/s and reaches a nadir of 48.81 Hz before stabilizing after 16 s at the level of 49.55 Hz. The latter response is out of the acceptable normal operating state bounds set by TSOs. For this reason, the provision of FFS by other synthetic inertia means should be examined. Also, it is clear that due to the decoupling of the areas via the MMC-based HVDC links the frequency in the neighboring areas is not affected as the APG controller of the HVDC links is not activated.

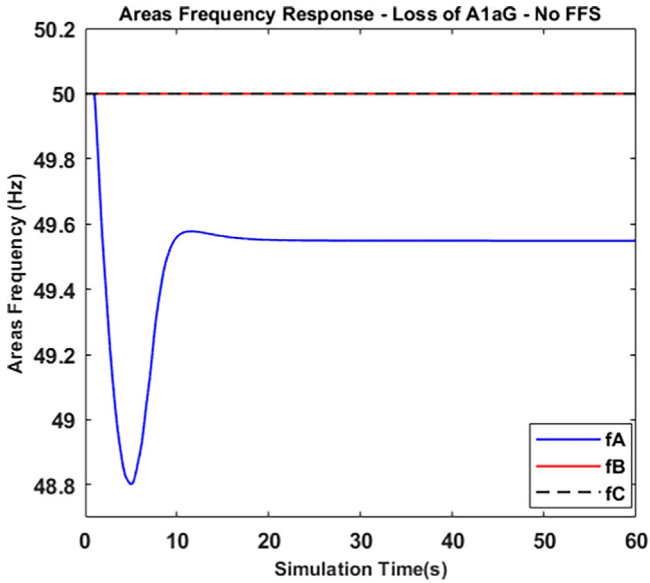

Fig. 14 Areas' frequency responses—loss of SGU A1aG—no FFS.

10.6.3.2 Scenario 2

In the second scenario, FFS is provided by the local electrolyzers installed in the affected area. The hydrogen-based units are set to operate at their maximum ramp rate capability injecting active power at 0.5 pu/s, which as explained in Section 10.2 is the minimum expected maximum ramp rate for large units. Electrolyzers may have different available bids for FFS, which may correspond to 30%, 50%, or 70% of their installed capacity. The frequency response of the affected area in case each of the different bids is provided and can be observed in Fig. 15. The electrolyzers can change their consumption according to the instantaneously measured Δf and provide their support for an unlimited amount of time. As it can be observed, as the bid of the electrolyzers increases, better frequency responses are obtained. In fact, the available bid due to the rapid response capability may lead to significantly improved nadirs from 48.81 Hz to 49.45 Hz, improved RoCofs and faster stabilization to a level up to 49.74 Hz. However, even at the best-case scenario, the frequency response does not fulfill the normal operating state bounds. Also, it is important to be mentioned that the frequency in the other areas remains constant at 50 Hz due to the decoupling achieved with the introduction of the MMC-HVDC links.

10.6.3.3 Scenario 3

In this scenario, all the three interconnected areas are activated to provide FFS to the affected area by modifying the power flows of the MMC-HVDC links 0.3 s following an active power imbalance once per simulation. The electrolyzers installed in all areas

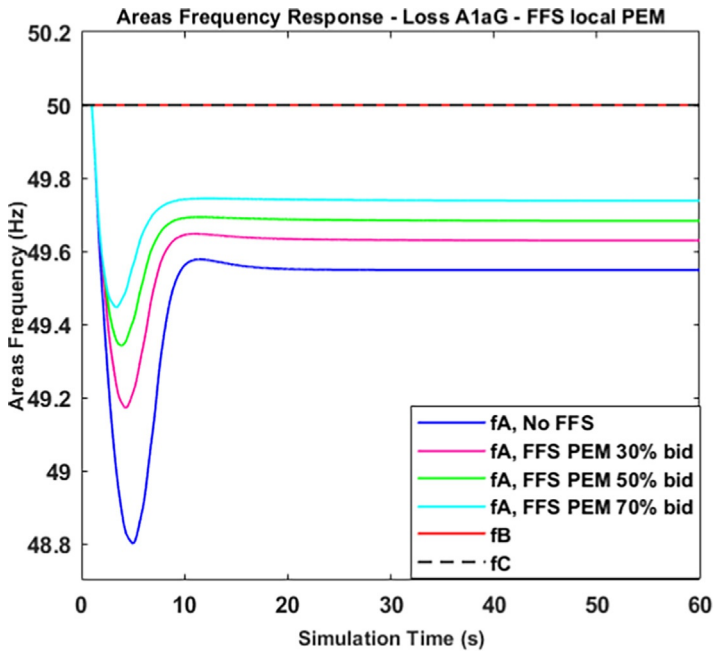

Fig. 15 Areas' frequency responses—loss of SGU A1aG—FFS by local PEM electrolyzers.

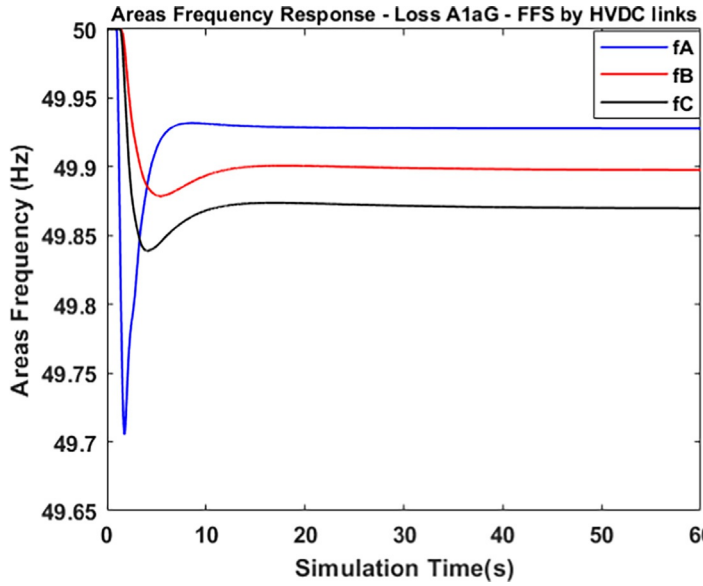

Fig. 16 Areas' frequency responses—loss of SGU A1aG—FFS by MMC-based HVDC links.

are assumed to have constant consumptions and not to participate in the frequency regulation. The participation of the HVDC links in the regulation is determined according to the solution of the optimization problem defined in Section 10.3 with the aid of the MVMO algorithm, aiming at the improvement of the frequency response in the affected area with the minimum impact on the interconnected areas. Having performed a series of 100 iterations, the frequency responses of the interconnected areas following the loss of the SGU A1aG at the first second of simulation can be observed in Fig. 16.

In this case due to the response of the HVDC links to the sensed imbalance, the frequency in all 3 interconnected areas is affected. Initially, area A, the affected area, experiences a rapid drop in its frequency according to the natural inertia characteristics of the area as no means of synthetic inertia are activated to support. After 0.3 s, the HVDC links alter their power flows to support the affected area, leading to smaller in size active power imbalances in the other areas sensed at the CCPs of the HVDC links. In this scenario, it can be observed that the frequency in area A drops to 49.71 Hz, a significantly improved nadir compared to the other scenarios and stabilizes at 49.93 Hz. The frequency in the other areas drops to 49.84 Hz and 49.88 Hz initially before restoring to 49.87 Hz and 49.9 Hz, respectively, for areas C and B. In that way, all the 3 interconnected areas have their frequencies within the normal operating state bounds and are able to cooperatively arrest the loss of the largest generating unit in the area with the lowest inertia conditions. Also, in this case as observed in Fig. **17**, HVDC link AB is the one that experiences the most significant change from 600 MW to 150 MW reducing the exports from area A to B, whereas the drop in HVDC link AC is smaller in size. That is due to the fact that area B has larger inertia compared to C

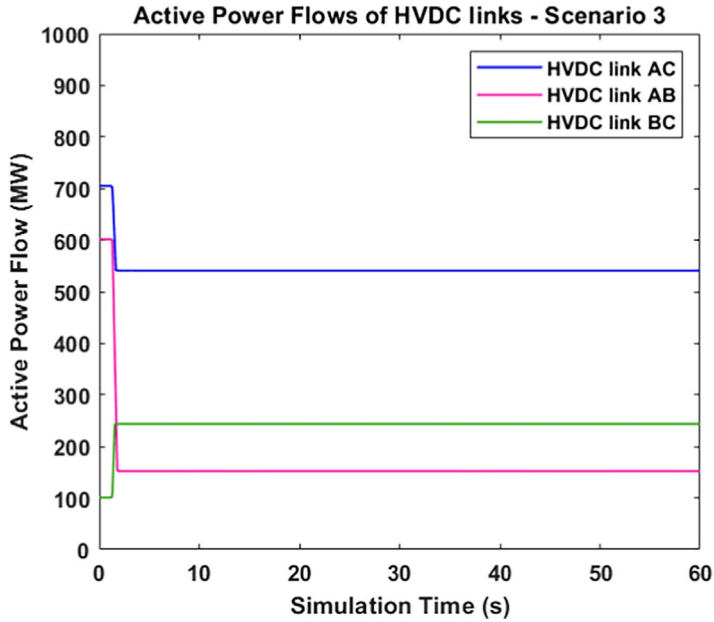

Fig. 17 HVDC links response—Scenario 3.

and thus it is able to sustain more abrupt and large active power imbalances. Then link BC tries to mitigate the imbalance and optimally share it among the 3 areas.

10.6.3.4 Scenario 4

In this case, all the different means of synthetic inertia in all the three areas are cooperatively tuned against the loss of SGU A1aG to mitigate the frequency excursions encountered. The participation of each unit in terms of magnitude and rate is determined according to the solution of the optimization problem in Section 10.3, trying to minimize the frequency excursions in all areas throughout the whole simulation period. Following the predefined number of iterations, the best frequency responses of the 3 interconnected areas can be observed in Fig. 18. As it is clear in this case, the best frequency responses among the examined scenarios are obtained in terms or frequency nadir, steady-state deviation, RoCof and time to stabilize. Area A, after the initial drop due to the disturbance very quickly recovers almost to 49.97 Hz and the frequency in the other areas never drops below 49.9 Hz, effectively preserving in within the normal operating state limits even at the worst expected simulation event. Area B, the area with the largest inertia level is the one that mainly shoulders the support of the affected area due to its characteristics.

In the response of the HVDC links, shown in Fig. 19, it can be also observed that both links AC and AB rapidly reduce the exports from area A to sustain the frequency deviation 0.3 s after its occurrence. In the meantime, the electrolyzers of area A are responsible when triggered to arrest the initial frequency drop until the activation of the other supporting means. When then the imbalance is shared to the other areas,

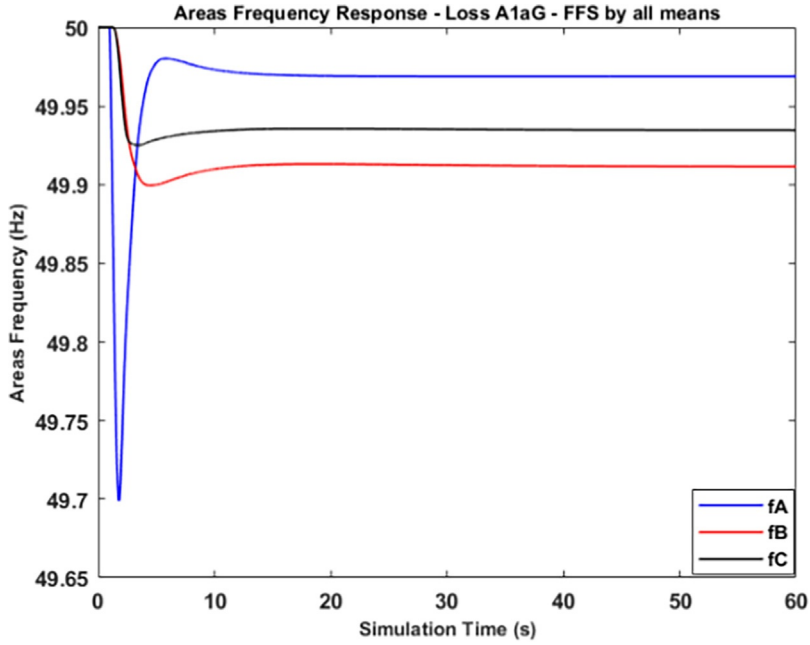

Fig. 18 Areas' frequency responses—loss of SGU A1aG—FFS by all means of SI.

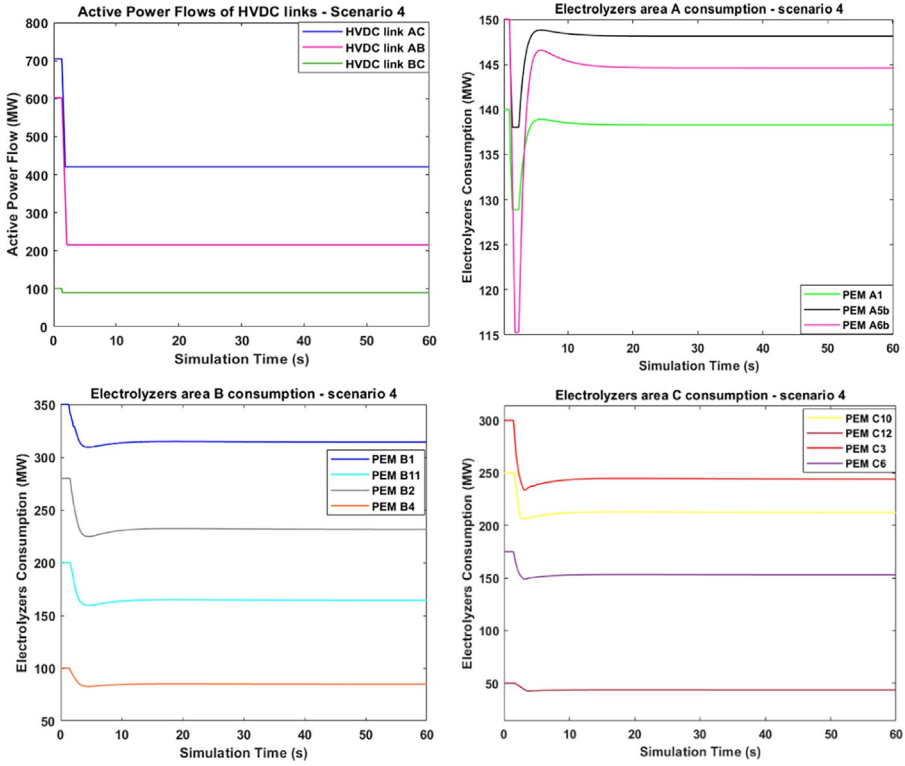

Fig. 19 HVDC links and PEM electrolyzers response—Scenario 4.

PEM electrolyzers are also activated to provide their support with respect to their capacity and location of installation with respect either to the location of the disturbance or the CCP of the HVDC link which shares the imbalance. Units installed closer to the CCPs are more significantly affected as observed in Fig. 19. Finally, in this scenario, the frequency in all areas smoothly recovers to a new level, whereas the consumption of the electrolyzers stabilizes at a new equilibrium point due to their capability to offer unlimited in time support and HVDC links operate according to their new active power setpoints. Hence, the solution of the optimization problem has provided the tuning parameters to achieve a new stable operating point having shared the imbalance among the different FFS units according to their characteristics, capabilities, and location of installation.

10.7 Discussion

In the previous sections, it has been revealed that the transformation of the power systems into power electronics dominated power systems may lead to challenges with respect to their frequency stability. As a result, in the case of a 3-area hybrid HVDC-HVAC system, the loss of the largest generating unit in the area with the lowest inertia conditions may trigger the frequency out of the acceptable limits as shown in Scenario 1 if no support is provided by PEI units. The utilization of local responsive demand units installed on various locations of the affected area representing in total the 20% of the local demand may significantly improve the response of the system especially when PEM electrolyzers are considered. However, as it has been shown in Scenario 2, the available bid of these reserve units plays an important role in the response of the system even at the most rapid adjustment of the consumption of the latter units. For this reason, the participation of other neighboring areas with the aid of the control systems of the HVDC links is more than necessary. In that case, even if the PEM electrolyzers are not considered, a coordinated tuning of the controllers is more than necessary to determine the degree of participation of each FCR to avoid adverse control actions such as insufficient or over frequency regulation and always taking into consideration the technical limitations of each element. Scenario 3 has shown that a simple modification of the power flows of the HVDC links can effectively achieve significantly improved frequency responses being tuned with the aid of MVMO under the proposed problem formulation. The frequency in all interconnected areas remains within the acceptable normal operating state limits and achieves a smaller value of the OF in (1) compared to other scenarios as shown in Table 4. The latter means that both the frequency response in the affected area improves but also the impact on the other areas shrinks. Also, from the OF value it can be observed that the total impact in all the 3 areas in Scenario 3 is smaller than the total impact in Scenarios 1 and 2 even through only area A is affected in Scenarios 1 and 2. In any case, Scenario 4 where all the different elements (PEM electrolyzers and HVDC links) are cooperatively tuned against the same imbalance with the aid of MVMO algorithm achieves the best frequency responses. That it is clear in Fig. 20 where the frequency response of the affected area is observed in each scenario and

Table 4 Simulation results.

Scenario	OF value	f_{A_nadir} (Hz)	$f_{A\_Steady\text{-}state}$ (Hz)	Time to stabilize
1	16.468	48.81	49.55	20
2a	9.782	49.17	49.63	17
2b	6.904	49.34	49.68	16
2c	4.715	49.45	49.74	14
3	2.006	49.71	49.93	12
4	0.843	49.71	49.97	11

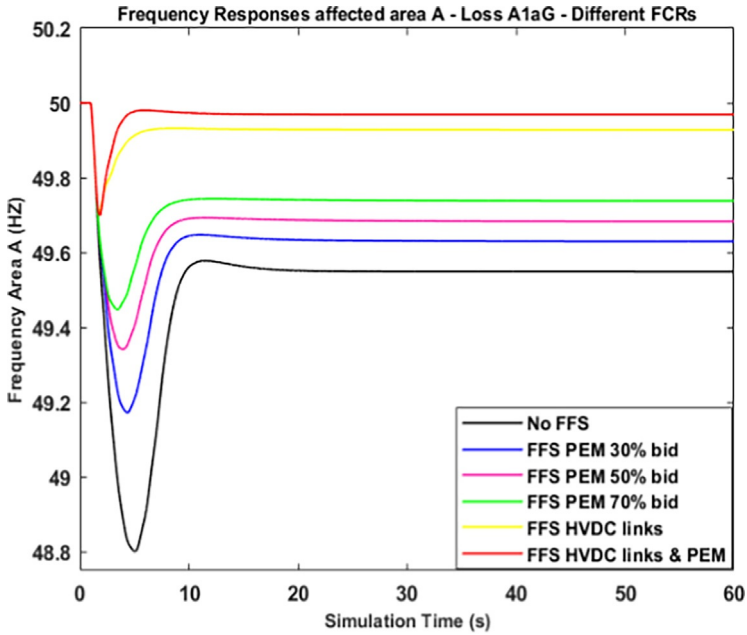

Fig. 20 Frequency response of the affected area—loss of SGU A1aG—different scenarios.

in Table 4 where the detailed results are presented. The best frequency response in terms of nadir, RoCof, steady-state deviation, and stabilization time but also the minimum OF value and impact on neighboring areas is obtained under Scenario 4. What is also important to be mentioned is that the location of installation of the various FCRs plays a significant role in the frequency regulation in accordance to their capacity and ramp rate as units closer to the disturbance of close to the CCPs of the HVDC links that share the imbalance to supporting areas are more critically affected.

The proposed problem formulation can be effectively used to tune the frequency controllers, considering the total frequency response of the system and being easily applicable to any system as it is based on the frequency measurement. However, the simulation time selected may influence its performance as a smaller simulation time leads to focus more on the transient period, whereas a larger simulation time leads to focus on the steady-state deviation. The MVMO algorithm used for the

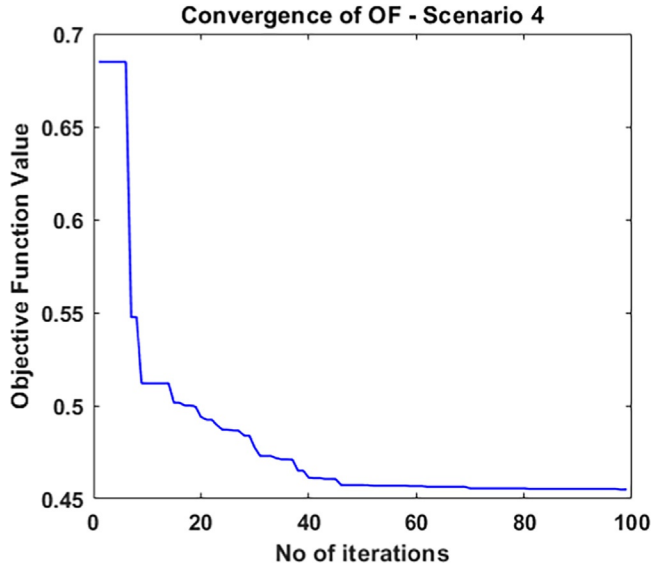

Fig. 21 Objective function convergence—Scenario 4.

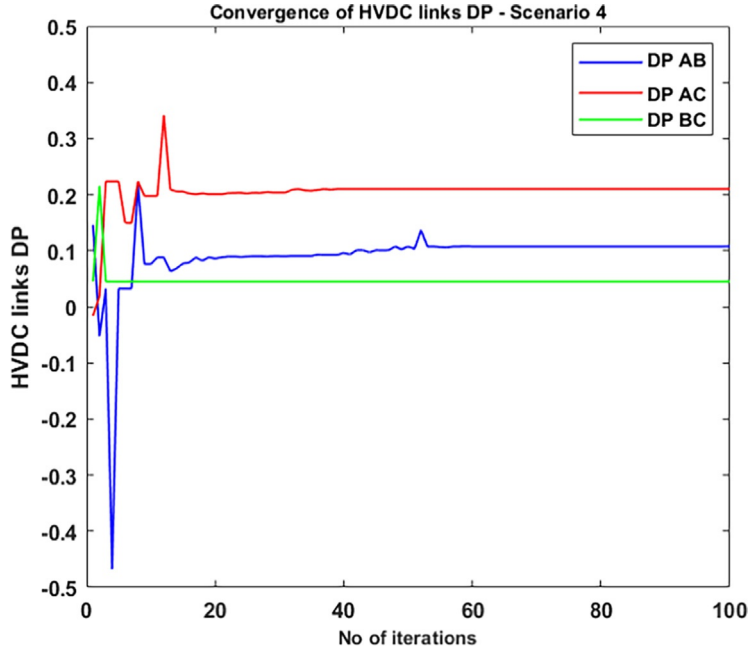

Fig. 22 Optimization variables convergence—Scenario 4—HVDC links DP.

solution of the optimization problem has shown very fast convergence rates as it able to reach an acceptable local optimum solution within a very short number of iterations as it can be observed in Fig. 21. Finally, Fig. 22 and 23 show the convergence of the amount of additional power provided by HVDC links and PEM electrolyzers,

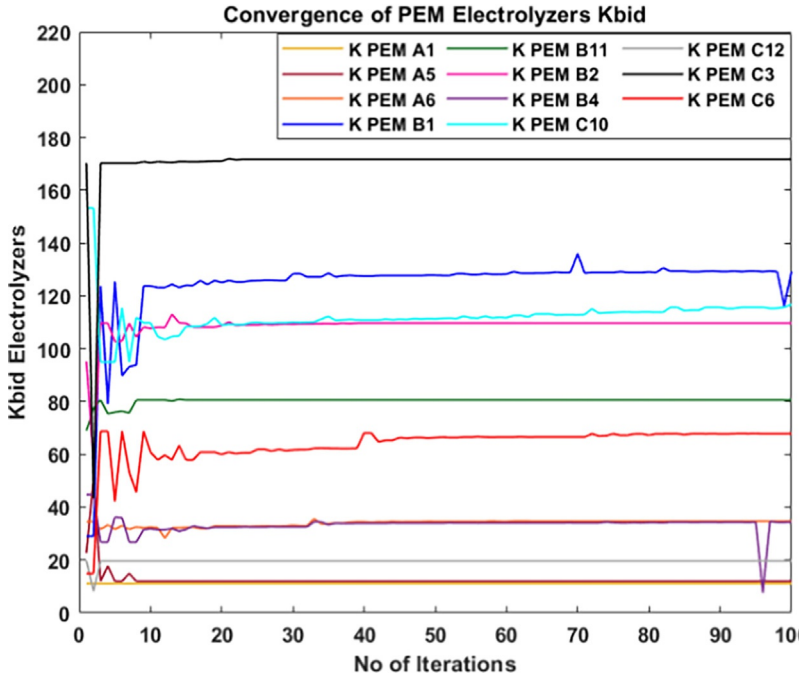

Fig. 23 Optimization variables convergence—Scenario 4—PEM electrolyzers bid.

respectively. As it is clear HVDC links that are directly interconnected with the affected area are more significantly affected and thus they appear to need more iterations to converge to an optimum level. That influences also the participation of the electrolyzers. As it can be seen in Fig. 23, the units installed closer to the CCPs of the HVDC links in the supporting areas are contributing more to the minimization of the impact in these areas according always to their capacity. On the other hand, PEM electrolyzers in the affected area are only responsible for the first ms following the disturbance to arrest the initial drop and then the regulation is mainly shouldered by the HVDC links which have higher transfer capability. That reveals the necessity for sophisticated constraints in the MVMO algorithm to utilize the local FCRs first before affecting other areas.

10.8 Conclusions

The introduction of PEI elements into the grid has significantly altered the response of the system to active power imbalances due to the new operating conditions, the structure of the system, and the characteristics of the new elements. For this reason, the control systems of the PEI units should improve and cooperate to shoulder the frequency regulation and enhance the stability margins of the system.

In this chapter, a coordinated FFS method taking advantage of the APG control scheme attached to MMC-based HVDC links and PEM electrolyzers has been

proposed. In fact, a 3-area highly meshed power system has been modified to facilitate the introduction of MMC-based HVDC links in replacement of the weak HVAC tie-lines and PEM electrolyzers representing the 20% of the local demand of each area. For the modeling of these elements, representative models for dynamic stability studies proposed in literature have been deployed. Also, the control structures of the MMC converters and the PEM electrolyzers have been modified so as to include the APG control block which is able to control the amount of additional power injected/absorbed from these units and the ramp rate the change in their active power output occurs in a coordinated way. The coordination of the control structures of the installed FCRs is achieved with the cooperative tuning of the controllers based on the solution of an optimization problem aiming at the minimization of the frequency excursions in the interconnected areas participating in the regulation following a commonly occurred active power imbalance. The optimization problem has been programmed in Python 3.8 along with the MVMO algorithm utilized for its solution and performs in a co-simulation environment with DPF 2020 where a series of time domain RMS simulations is performed to obtain the frequency responses of the system.

To test the effectiveness of the proposed strategy, a simulation event leading to the loss of the largest generating unit in the area with the lowest inertia conditions has been considered under different simulation scenarios where different groups of FCRs are activated to provide FFS. The simulation results have initially proven the fact that the transformation of the system can significantly affect its frequency stability and that the PEI units can effectively improve it utilizing the APG control scheme. The proposed problem formulation can be effectively used to tune the controllers of MMC-based HVDC links and PEM electrolyzers and achieve a frequency response within the normal operating state limits even at the worse case scenarios. Also, it is easily applicable to any system as it is based on the frequency measurement that can be obtained at any bus of each area. However, special attention needs to be paid in the areas prioritization through the weighting factors and in the selection of the simulation time. Furthermore, it can be concluded that the more the available FCRs, the better the frequency response of the system as different units with special response characteristics and installed at different critical locations can be effectively cooperate with the aid of the MVMO algorithm to achieve the optimal results both for the affected and the supporting areas.

This chapter is related with the field of coordinated fast frequency support from power electronic interfaced units installed at generation, demand, and transmission sides. Further research will be devoted in the optimal tuning methods of the frequency controllers of multiple units operating at all different sides in complex multiarea, multienergy, hybrid HVAC/HVDC power systems.

References

[1] A. Halley, N. Martins, P. Gomes, D. Jacobson, W. Sattinger, Y. Fang, L. Haarla, Z. Emin, M. Val Escudero, S. Almeida De Graaff, V. Sewdien, A. Bose, Effects of increasing power electronics-based technology on power system stability: Performance and operations, CIGRE Sci. Eng. 11 (June 2018) 5–17.

[2] N. Hatziargyriou, J.V. Milanović, C. Rahmann, V. Ajjarapu, C.A. Canizares, I. Erlich, D.J. Hill, I. Hiskens, I. Kamwa, B.C. Pal, P. Pourbeik, J.J. Sanchez-Gasca, A.M. Stankovic, T. Van Cutsem, V. Vittal and C. Vournas, Stability definitions and characterization of dynamic behavior in systems with high penetration of power electronic interfaced technologies, IEEE Power and Energy Society, Tech. Rep. PES-TR77, May 2020 (Available on-line: https://resourcecenter.ieeepes.org/technical-publications/technicalreports/PES_TP_TR77_PSDP_stability_051320.html).

[3] N. Hatziargyriou, J.V. Milanović, C. Rahmann, V. Ajjarapu, C. Cañizares, I. Erlich, D. Hill, I. Hiskens, I. Kamwa, B. Pal, P. Pourbeik, J.J. Sanchez- Gasca, A. Stanković, T. Van Cutsem, V. Vittal and C. Vournas: "Definition and classification of power system stability—revised and extended", IEEE Trans. Power Syst., December 2020.

[4] L. Meegahapola, A. Sguarezi, J.S. Bryant, M. Gu, D.E.R. Conde, R.B.A. Cunha, Power system stability with power-electronic converter interfaced renewable power generation: present issues and future trends, Energies 13 (2020) 3441, https://doi.org/10.3390/en13133441.

[5] V.N. Sewdien, R. Chatterjee, M. Val Escudero, and J. Van Putten, System operational challenges from the energy transition, CIGRE Sci. Eng., vol. 17, pp. 5-19, Feb. 2020.

[6] E. Rakhshani, A. Perilla, J.L.R. Torres, F.M. Gonzalez-Longatt, T.B. Soeiro, M.A.M.M. Van Der Meijden, FAPI controller for frequency support in low-inertia power systems, IEEE Open Access J. Power Energy 7 (2020) 276–286, https://doi.org/10.1109/OAJPE.2020.3010224.

[7] E. Rakhshani, J.L. Rueda Torres, P. Palensky, M.D. van Meijden, Determination of maximum wind power penetration considering wind turbine fast frequency response, in: 2019 IEEE Milan PowerTech, 2019, pp. 1–6, https://doi.org/10.1109/PTC.2019.8810492.

[8] E. Rakhshani, D. Gusain, V. Sewdien, J.L. Rueda Torres, M.A.M.M. Van Der Meijden, A key performance indicator to assess the frequency stability of wind generation dominated power system, IEEE Access 7 (2019) 130957–130969, https://doi.org/10.1109/ACCESS.2019.2940648.

[9] C. Zhang, E. Rakhshani, N. Veerakumar, J.L.R. Torres, P. Palensky, Modeling and optimal tuning of hybrid ESS supporting fast active power regulation of fully decoupled wind power generators, IEEE Access 9 (2021) 46409–46421, https://doi.org/10.1109/ACCESS.2021.3066134.

[10] N. Sharma, S. Sankar, Modeling and control of battery energy storage system for providing grid support services, in: 2018 Clemson University Power Systems Conference (PSC), 2018, pp. 1–5, https://doi.org/10.1109/PSC.2018.8664018.

[11] A.D. Perilla Guerra, J.L. Rueda Torres, A.A. van der Meer, M.A.M.M. van den Meijden, A. Alefragkis, Influence of active power gradient control of an MMC-HVDC link on long-term frequency stability, in: 2017 IEEE Power & Energy Society General Meeting, Chicago, IL, USA, 2017.

[12] J.L. Rueda Torres, A.D. Perilla Guerra, E. Rakhshani, P. Palensky, M.A.M.M. van der Meijden, A. Alefragkis, MVMO-based tuning of active power gradient control of VSC-HVDC links for frequency support, in: 2019 2nd International Conference on Smart Grid and Renewable Energy (SGRE), Doha, Qatar, 2019.

[13] A.D. Perilla Guerra, D. Gusain, J.L. Rueda Torres, P. Palensky, M.A.M.M. van der Meijden, F. Gonzalez-Longatt, Optimal tuning of active power control for frequency support in multi-energy systems, in: 2020 IEEE PES Innovative Smart Grid Technologies Europe (ISGT-Europe), The Hague, The Netherlands, October 2020.

[14] F. Alshehri, V.G. Suarez, J.L. Rueda Torres, A.D. Perilla Guerra, M.A.M.M. van der Meijden, Modelling and evaluation of PEM hydrogen technologies for frequency ancillary services in future multi-energy sustainable power systems, Heliyon 5 (2019), e01396.

[15] P. Ayivor, J.L. Rueda Torres, M.A.M.M. van der Meijden, R. van der Pluijm, B. Stouwie, Modelling of large size electrolyzer for electrical grid stability studies in real time digital simulation, in: Proceedings of Energynautics 3rd International Hybrid Power Systems Workshop, Tenerife, Spain, May 2018.
[16] TSO, Stability analysis of an international electricity system connected to regional local sustainable gas systems, in: TSO 2020 Activity 2 Final Report, 2019.
[17] N. Veerakumar, Z. Ahmad, M. Ebrahim Adabi, J.L. Rueda Torres, P. Palensky, M.A.M.M. van der Meijden, F. Gonzalez-Longatt, Fast active power—frequency support methods in large scale electrolyzers for multi-energy systems, in: 2020 IEEE PES Innovative Smart Grid Technologies Europe (ISGT-Europe), The Hague, The Netherlands, October 2020.
[18] W. Wang, A. Beddard, M. Barnes, O. Marjanovic, Analysis of Active Power Control for VSC HVDC, IEEE Trans. Power Deliv. 29 (4) (2014) 1978–1988.
[19] F. Sanchez, F. Gonzalez Longatt, D. Bogdanov, Probabilistic assessment of enhanced frequency response services using real frequency time series, in: 20th International Symposium on Electrical Apparatus and Technologies (SIELA), 2018, pp. 1–4.
[20] DIgSILENT GmbH, PowerFactory Seminar HVDC and Facts, Tech. Rep., DIgSILENT GmbH, Gomaringen, Germany, June 2018.
[21] CIGRE Working Group B4.57, "Guide for the Development of Models for HVDC Converters in a HVDC Grid", CIGRE, Tech. Rep., December 2014.
[22] J. Peralta, H. Saad, S. Dennetire, J. Mahseredjian, S. Nguefeu, "Detailed and Averaged Models for a 401-Level MMC-HVDC System", IEEE Trans. Power Deliv., vol. 27, no. 3, pp. 1501-1508, July 2012.
[23] H. Saad, S. Dennetire, J. Mahseredjian, P. Delarue, C. Guillaud, J. Peralta and S. Nguefeu, "Modular multilevel converter models for electromagnetic transients", IEEE Trans. Power Deliv., vol. 29, no. 3, pp. 1481-1489, June 2014.
[24] N. Flourentzou, V.G. Agelidis and G.D. Demetriades, "VSC-based HVDC power transmission systems: an overview, " in IEEE Trans. Power Electron., vol. 24, no. 3, pp. 592-602, March 2009, https://doi.org/10.1109/TPEL.2008.2008441.
[25] Z.B. Ibrahim, M.L. Hossain, I.B. Bugis, N.M.N. Mahadi, A. Shukri, A. Hasim, Simulation investigation of SPWM, THIPWM and SVPWM techniques for three phase voltage source inverter, Int. J. Power Electron. Drive Syst. (IJPEDS) 4 (2) (January 2014).
[26] N.T. Trinh, M. Zeller, K. Wuerflinger and I. Erlich, "Generic model of MMC-VSC-HVDC for interaction study with AC power system", IEEE Trans. Power Syst., vol. 31, no. 1, pp. 27-34, Jan. 2016.
[27] A. Korompili, Q. Wu and H. Zhao, "Review of VSC HVDC connection for offshore wind power integration", Renew. Sustain. Energy Rev., vol. 59, pp. 1405-1414, June 2016.
[28] Hydrogen Council, Hydrogen scaling up—a sustainable pathway for the global energy transition, Hydrogen Council Tech. Rep., Nov. 2017.
[29] S.S. Kumar and V. Himabindu, "Hydrogen production by PEM water electrolysis—a review", Mater. Sci. Energy Technol. 2, pp. 442-454, March 2019.
[30] B.W. Tuinema, E. Adabi, P.K.S. Ayivor, V. Garcia Suarez, L. Liu, A.D. Perilla Guerra, Z. Ahmad, J.L. Rueda Torres, M.A.M.M. van der Meijden, P. Palensky, Modelling of large-sized electrolysers for real-time simulation and study of the possibility of frequency support by electrolysers, IET Generat. Trans. Distrib. 14 (10) (13 May 2020) 1985–1992.
[31] T.S.O.B.V. Tennet, FCR Manual for BSPs: Requirements and procedures for supply of FCR, in: Tech. Rep. TenneT TSO B.V., The Netherlands, 2020.
[32] European Commission, Commission Regulation (EU) 2017/1485 of 2 August 2017 establishing a guideline on electricity transmission system operation, European Commission, Brussels, 2017.

[33] European Commission, Commission Regulation (EU) 2017/2196 of 24 November 2017 establishing a network code on electricity emergency and restoration, European Commission, Brussels, 2017.
[34] J.L. Rueda Torres, I. Erlich, Hybrid Single Parent-Offspring MVMO for Solving CEC2018 Computationally Expensive Problems, in: 2018 IEEE World Congress on Computational Intelligence, Rio de Janeiro Brazil, July 2018, pp. 1–8.
[35] S.P. Teeuwsen, Phd Dissertation, Oscillatory Stability Assessment of Power Systems using Computational Intelligence, Technische Universitat Duisburg-Essen, Germany, 2005.
[36] F.M. Gonzalez-Longatt, J.L. Rueda Torres, PowerFactory Applications for Power System Analysis, Springer, Delft, The Netherlands, 2014.
[37] IEEE Standards Association, 1110-2019 IEEE Guide for Synchronous Generator Modelling Practices and Parameter Verification with Applications in Power System Stability Analyses, IEEE, March 2020.
[38] DIgSILENT GmbH, Technical Reference Synchronous Machine PowerFactory 2020, in: DIgSILENT Tech. Rep., Gomaringen Germany, February 2020.
[39] P. Kundur, Power System Stability and Control, first ed., McGraw-Hill Professional, 1994.
[40] IEEE Standards Association, IEEE Recommended Practive for Excitation System Models for Power System Stability Studies (IEEE Std 421.5-2016), IEEE, New York, USA, 2016.
[41] IEEE Power System Dynamic Performance Committee, Power System Stability Subcommittee, Task Force on Turbine-Governor Modelling, in: Dynamic Models for Turbine-Governors in Power System Studies (PES-TR1 Tech. Rep.), IEEE, January 2013.